Int j simul model 21 (2022) 4, 579-590
Original scientific paper

ASSESSMENT OF ASYMMETRICAL STRESS PROFILE WITHIN WOOD USING RESTORING FORCE TECHNIQUE

Leelatanon, S.[*,#]; Jantawee, S.[**]; Vannarat, S.[***] & Matan, N.[*,****]

[*] Centre of Excellence in Wood and Biomaterials, School of Engineering and Technology, Walailak University, Thasala, Nakhon Si Thammarat 80160, Thailand

[**] Faculty of Industrial Technology, Nakhon Si Thammarat Rajabhat University, Meaung, Nakhon Si Thammarat 80280, Thailand

[***] Institute for Promotion of Teaching Science and Technology, 924 Sukhumvit Road, Phra Khanong, Khlong Toei, Bangkok 10110, Thailand

[****] Centre of Excellence on Petrochemical and Materials Technology, Chulalongkorn University, Bangkok, Thailand

E-Mail: lsatjapa@wu.ac.th ([#] Corresponding author)

Abstract

Asymmetrical internal stress profile within the kiln-dried lumber assessed using the restoring force technique on the half-split specimen has been investigated. Unlike the symmetrical internal stress profile in which the measured restoring force is completely described by an elastic beam theory, the asymmetrical internal stress profile also induces a so-called remnant force. By using the released strain and the elastic modulus data across the entire thickness obtained from the McMillen slice test, a numerical result based on the finite element model successfully simulates the restoring force profile for an entire range of both symmetric and asymmetric stress profiles. The finite element model is leveraged to evaluate the effect of asymmetry of stress profile on the remnant force. The value of the remnant force linearly depends on the stress profile deviation which is inferred to the level of asymmetric stress profile.
(Received in July 2022, accepted in September 2022. This paper was with the authors 2 weeks for 1 revision.)

Key Words: Stress Assessment, Finite Element Model, Elastic Beam Theory, Asymmetrical Stress Profile, Wooden Specimen

1. INTRODUCTION

Internal stress is developed inside wood as a result of a differential shrinkage in the surface and the core sections of lumber during drying. This induced stress can cause cracking, warping and cupping in lumbers [1]. In addition to the differential shrinkage, even when one considers the drying stress in a single direction of a symmetric cross section of lumber, the drying stress profile in the same plane might be asymmetrical [2, 3]. This is because the drying stress caused by shrinkage depends upon several parameters including the location of lumber in a tree trunk, juvenile and mature wood, fibre orientation, sawing pattern, cutting direction, moisture content, modulus of elasticity, and shrinkage coefficient [4-6].

The conventional techniques, the prong test and the McMillen slice test, are typically used to measure the deformation and internal stress in a wood cross section caused by drying. In many research papers, these techniques showed the asymmetrical deformation and stress profile of the cross section [2]. The deformation and the internal stress on both sides of a single plane, left and right, were not exactly symmetric. It has to be noted that, additionally, those techniques could not measure the internal stress directly. They only measure the deformation or the strain, so testing of modulus is still required if one would like to know the stress.

Recently, a novel assessment of the internal stress has been developed using the force-based method called the restoring force technique firstly developed by Diawanich et al. [7] and later improved by Jantawee et al. [8]. The technique was able to measure the internal stress in kiln-dried lumbers by clamping a wood sample onto the steel frame. The sample was cut along the

half-split length by a band saw. The sample was deformed due to the compressive stress and the tensile stress in the surface and the core layer respectively. The force induced by the stress relaxation which was needed to keep the sample in the original position was transferred to the load cell, and it was monitored so called the restoring force. Also, the equation relating the restoring force and the internal stress has been proposed. Interestingly, the proposed equation requires only the geometrical parameter of the test sample without knowing of modulus [8].

The restoring force technique has been employed to examine the kiln-dried lumbers [8]. It appeared that a lot of measured restoring force profiles could not entirely be explained by the analytical model derived from an elastic beam theory [9]. Without a clear explanation, an additional remnant force obtained by extrapolation of the cutting length to infinity must be incorporated into the analytical model to completely describe the restoring force profile.

This research contributes to discover the effect of the asymmetrical profile of drying stress of wood on the existence of the remnant force. The validated simulation model of finite element (FE) analysis is leveraged to evaluate the degree of asymmetry of stress profile on the quantity of the remnant force. This has not yet been studied by literature.

2. THE ANALYTICAL MODEL

The restoring force technique is basically developed from the beam theory. The linear distribution of internal stress is assumed across half thickness. The maximum stress is assumed to be equal at the outer surface and the inner core. This assumption has been proved by both experimental and numerical results proposed in the previous works [8-11]. The magnitude of maximum stress (σ_m) can be calculated by a deflection of the half-split specimen as expressed by:

$$\sigma_m = \frac{E \cdot \Delta\delta \cdot d}{4l^2} \tag{1}$$

where E, $\Delta\delta$, d and l are modulus of elasticity in the tangential direction, mouth opening, thickness and half-split length of the specimen, respectively [12]. The restoring force, P, required to keep the half-split specimen in the original position can be determined by:

$$P = \frac{E \cdot \Delta\delta \cdot b}{S} \tag{2}$$

where b is sample length and S is a geometrical shape factor [13]. By combining the common terms in Eqs. (1) and (2), the maximum stress can be calculated as:

$$P = \frac{4bl^2}{Sd}\sigma_m \tag{3}$$

According to Hibbeler [14], the deflection at the free end of a cantilever beam subjected to point load derived from the Euler–Bernoulli elastic beam theory can be calculated by:

$$\frac{\Delta\delta}{2} = \frac{P(l-g)^2}{6EI}\left(3l-(l-g)\right) \tag{4}$$

where g is the distance of the clamping screw from the top end of the specimen and I is the moment of inertia. By substituting $I = bd^3/96$ into Eq. (4) and combining Eqs. (2) and (4), the geometrical shape factor can be expressed as:

$$S = \frac{32\left(l-g\right)^2\left(2l+g\right)}{d^3} \tag{5}$$

Using Eq. (3) together with Eq. (5) demonstrates that the internal stress can be determined by the measured force and the geometric shape factor. Most importantly, there is no need for the modulus of elasticity in the calculation.

According to Leelatanon et al. [9], typical plots P against the term $4bl^2/Sd$ still behave in flexural response for all the restoring force profiles but a positive y-intercept of the remnant force P_o is observed. Consequently, Eq. (3) has been suitably adapted as:

$$P = \frac{4bl^2}{Sd}\sigma_{\mathrm{m}} + P_o \tag{6}$$

Since the restoring force technique does not need the modulus of elasticity in the calculation, this technique is well suitable for measuring internal stress in wood in which the modulus of elasticity is not constant across the thickness depending on and temperature and moisture content [4-6]. However, this technique is not proper for materials that is easily broken such as ceramic because it is not flexible enough for force detection.

3. MATERIALS AND METHODS

3.1 Measurements of restoring force of symmetric and asymmetric drying stress profiles

The flat-sawn industrial kiln-dried rubberwood lumbers, the produce of 25- to 30- year-old rubber trees, were collected from a local sawmill in Nakhon Si Thammarat, Thailand. All rubberwood lumbers were produced to the commercial sizes for exporting overseas and there was no standard size for the restoring force technique. Therefore, the lumbers used in this research project were mainly focused on the most ordered size. The defect-free pieces of lumber were cut a meter long in the longitudinal direction to the grain. The lumbers had the thickness of 30 mm in the radial direction (d), and the width of 130 mm in the tangential direction (W). Before making the samples, one end of each lumber was cut out approximately 50 mm to get rid of the stress relaxation. Then, three adjacent pieces of 50 mm long (b) specimens were prepared to measure the restoring force, to measure the released strain tested by the McMillen slice method, and to measure the modulus of elasticity in the tangential direction to the grain of the wood as shown in Fig. 1 a. Three replicates of each lumber were examined [8].

The determination of restoring force was prepared according to Jantawee et al. [8]. The specimen was fixed onto the steel frame by the screws at a clamping distance of 10 mm (g) from the top of the specimen as shown in Fig. 1 b. The specimen clamped to the steel frame was cut at a half thickness in a wide direction along a half-split length (l) as presented in Figs. 1 b and 1 c. The restoring force was then recorded at every half-split length (l) of 5 mm intervals until the specimen was divided into two pieces or the crack was observed. For the McMillen slice test, the specimen was marked by divided lines so it could be cut into six-equal slices as shown in Fig. 1 d. Before slicing, the initial width of each slice (W_b) was measured by callipers having a precision of 0.01 mm. Each slice was marked the measurement location and its number so that the width measurements after slicing could be measured at the same location. The specimen was then sliced along the divided lines. Its width, W_a, was subsequently measured of each slice. After that, the released strain of each slice was calculated according to $\varepsilon = (W_a - W_b)/W_b$. Additionally, the modulus of elasticity in the tangential direction (E_T) of all slices were determined using a 150 kN universal testing machine (Lloyd, UK) connected with a strain gauge (Epsilon Technology, USA).

3.2 Finite element model of the restrained half-split specimen

Since the mechanical property of wood was orthotropic, the nine elastic constant in three mutually orthogonal materials should be assigned in the FE model [15, 16]. The validated FE model based on the previous works was used. The SOLID186 elements in ANSYS (v12, Ansys Inc., Pennsylvania, USA) were selected to generate the FE model to study the effect of the asymmetrical drying stress profile. The modulus of elasticity in the tangential direction (T) was fixed to a constant of 500 MPa, and all other moduli were calculated as ratios of the modulus

in tangential direction ($E_L : E_R : E_T = 20 : 1.6 : 1$, $G_{LR} : G_{LT} : G_{RT} = 10 : 9.4 : 1$ and $E_L : G_{LR} = 14 : 1$). Three Poisson's ratios were estimated to be μ_{RL} = 0.02, μ_{LT} = 0.02 and μ_{RT} = 0.35 based on values of tropical hardwood species [8-11, 15-18].

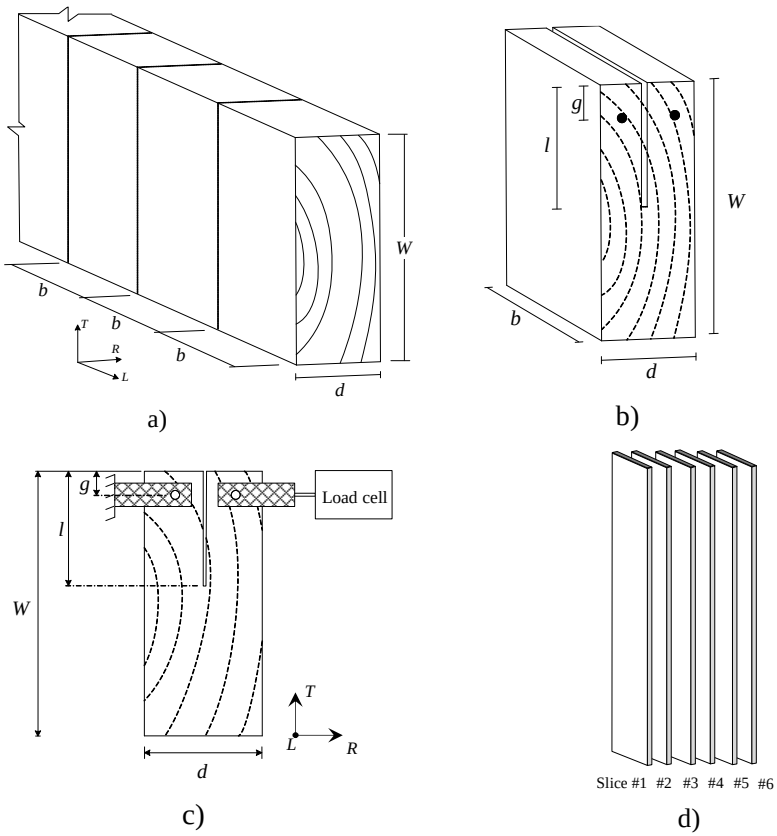

Figure 1: a) test specimen cut from the lumber board, b) half-split specimen for the restoring force measurement, c) diagram of the restoring force measuring apparatus, d) McMillen slice test.

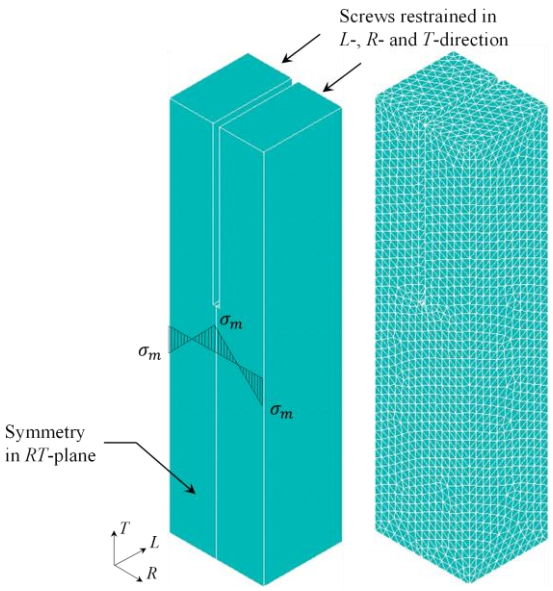

Figure 2: The 3D mesh of half of the specimen and boundary conditions used in FE simulation.

Only a half of the specimen was generated to reduce the computational time because the specimen had a plane of symmetry in the *RT*-plane as shown in Fig. 2. All nodes attached to the clamping screw area were restrained in the *L*-, *R*-, and *T*-direction to obtain the calculated

restoring force. The FE model was assigned the shrinkage due to temperature change to generate the initial conditions of the linear stress profile including the symmetric profile and the asymmetrical ones.

In addition, the FE model was used to verify the restoring force tested by the experiment. However, in this study, the released strain and the measured modulus in the *T*-direction of the specimen were applied to the layers that corresponded to the tests. All other moduli were assigned as ratios of the modulus of elasticity measured in the tangential direction as described previously.

4. RESULTS AND DISCUSSION

4.1 The effect of the asymmetrical drying stress profile on the restoring force

The maximum internal stress (σ_m) of the kiln-dried lumber can be evaluated using Eqs. (3) and (5) without knowledge of the modulus of wood. The restoring force should be proportional to the term $4bl^2/Sd$ with zero intercept ($P_o = 0$) at a relatively low value of $4bl^2/Sd$ or at a relatively long half-split length in the flexural range [8, 9]. However, this type of kiln-dried lumber was relatively rare. Typical plots of P against the term $4bl^2/Sd$ are different. The linear relationship between P and $4bl^2/Sd$ is still observed in the flexural response regime but with an additional value of a positive y-intercept ($P_o \neq 0$). Therefore, Eq. (3) has been modified to be Eq. (6) which includes both the dominant stress component in the tangential direction and the cumulative force due to the internal stresses in the other directions. Fig. 3 presents both a rare case ($P_o = 0$) and a typical case ($P_o \neq 0$) plot of P against the term $4bl^2/Sd$. The magnitude of σ_m and P_o of the rare case derived from the lower curve are 3.27 MPa and 0 N respectively, while those of the typical case obtained from the upper one are 2.90 MPa and 78.7 N respectively.

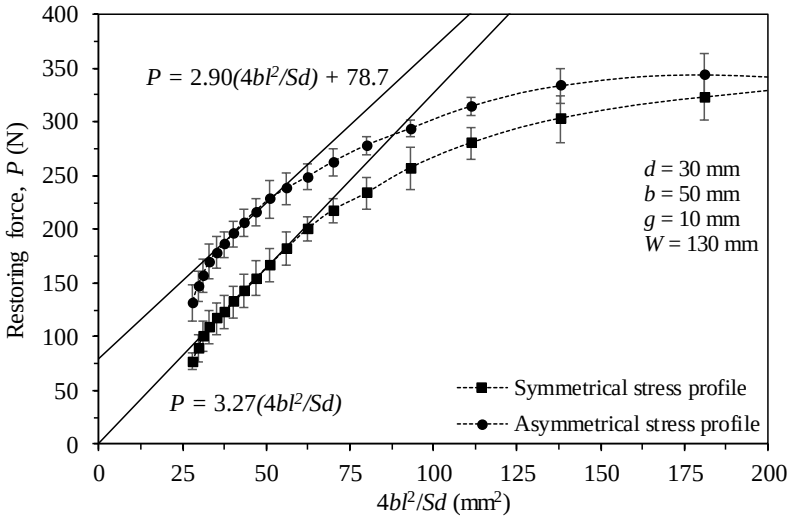

Figure 3: The restoring force *(P)* plotted against the term $4bl^2/Sd$ for $P_o \sim 0$ (Lower curve) and $P_o \neq 0$ (Upper curve); the solid straight lines show the best fits to the test data points in the flexural range.

The existence of the remnant force P_o after a relatively long half-split length is expected to be caused by the asymmetrical internal stress profile on the RT-plane of lumber. As observed in the symmetric drying stress profile (solid line) in Fig. 4, the maximum tensile stress was located right at the centre of the thickness, while the compressive stress on both surfaces had the same level. Differently, the location of the maximum tensile stress of the asymmetrical stress profile (dash line) deviated from the centre of the thickness, and the compressive stresses on both sides were not equal. Investigation of the possible origin of P_o using the finite element model is described in the following sections.

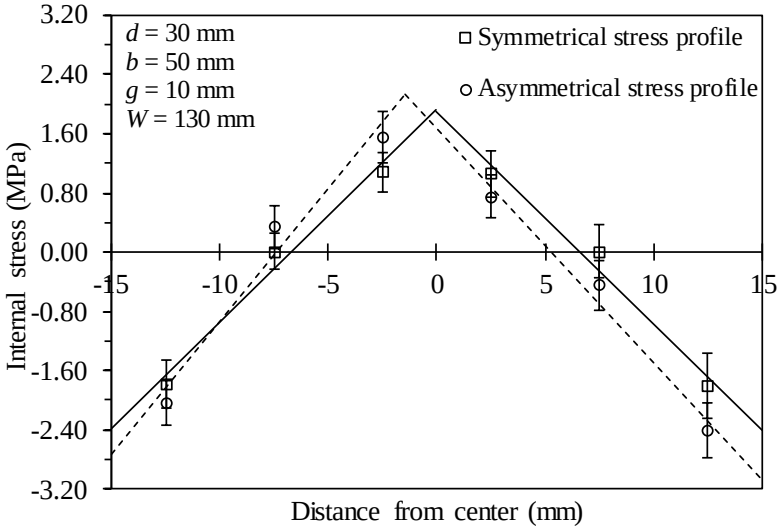

Figure 4: Distribution of the symmetric and asymmetric internal stress profiles with linear regression of internal stress profiles calculated from the slice test.

4.2 The validation of finite element model

The FE simulation was generated to calculate the restoring force of both the symmetric stress profile specimen ($P_o \sim 0$) and the asymmetrical stress profile specimen ($P_o \neq 0$) similar to those reported by Leelatanon et al. [9]. The modulus of elasticity (Fig. 5 a) and the released strain (Fig. 5 b) across the specimen thickness obtained by the tension test and the McMillan slice test respectively were the initial input of the FE models. The negative and positive released strain values were observed in the inner and outer sections of the specimen after slicing respectively caused by the tensile and compressive stresses remaining within the inner and outer sections. This mechanism has been declared for casehardening of kiln-dried lumber [19].

A reasonable agreement between the FE simulated restoring force and the measured restoring force patterns of the symmetric stress profile specimen is obtained for the entire profiles as shown in Fig. 6 a. Good agreement is also observed in the flexural range together with the calculated restoring force values according to the analytical model based on an elastic beam theory. However, the FE model appears to capture the restoring force behaviour at relatively short half-split lengths outside the flexural range where the analytical model has failed. The mechanical responses of both the FE result and the experimental one are similar to those reported by Leelatanon et al. [9]. An excellent agreement between the calculated and the measured restoring force values can be observed in the flexural range between the half-split lengths from 60 mm to 100 mm of the 130 mm wide specimens.

For the asymmetrical stress profile specimen ($P_o \neq 0$), using the modulus of elasticity and the released strain data in the width (tangential) direction across the thickness of the specimen as presented in Fig. 5 a and Fig. 5 b respectively, the FE simulated and measured restoring force profiles are plotted in Fig. 6 b. The magnitude of the simulated restoring force shows a good agreement with the measured restoring force similar to that observed in the symmetric stress profile specimen ($P_o = 0$). This is because the FE model in this study has been improved from that proposed by Leelatanon et al. [9]. The simulation in this study is applied the measured strain along the entire cross section of the specimen, so the asymmetry of the stress profile is taken into account. This is different from the previous model [9] where they used the average value of the released strain from both sides of the centre line and then applied it to a quarter of the specimen. This means the released strain applied to the FE model is always symmetric, so the asymmetry is lost by the averaging of strain data. Using the exact measured strain along the entire cross section, not the average, the FE model is able to capture both the restoring force at

the relatively short half-split lengths and at the flexural range. According to Eq. (6), the calculated restoring forces at those magnitudes of σ_m and P_o are compared with the experimental data in Fig. 6. An excellent agreement between the calculated and the measured restoring forces can be observed in the flexural range between the half-split lengths of 60 mm and 100 mm of the 130 mm wide specimens.

In both cases, symmetrical and asymmetrical stress profile, the magnitude of the calculated and the measured restoring force of the half-split lengths from 10 mm to 40 mm is obviously different. This is because the restoring forces calculated by Eqs. (3) and (6) are derived from the Euler–Bernoulli elastic beam theory. This theory is suitable for a long-span beam which corresponds to the half-split lengths between 60 mm to 100 mm. For a short-span beam, on the other hand, this beam theory is not fit to the half-split lengths between 10 mm and 40 mm. To explain the restoring force in the short-span length, the Timoshenko beam theory and the stress decay near free edges of a wood sample must be incorporated [11]. It has to be noted that, however, this paper mainly focusses on the restoring force and the remnant force in the long-span region where the Euler–Bernoulli elastic beam theory is adequate.

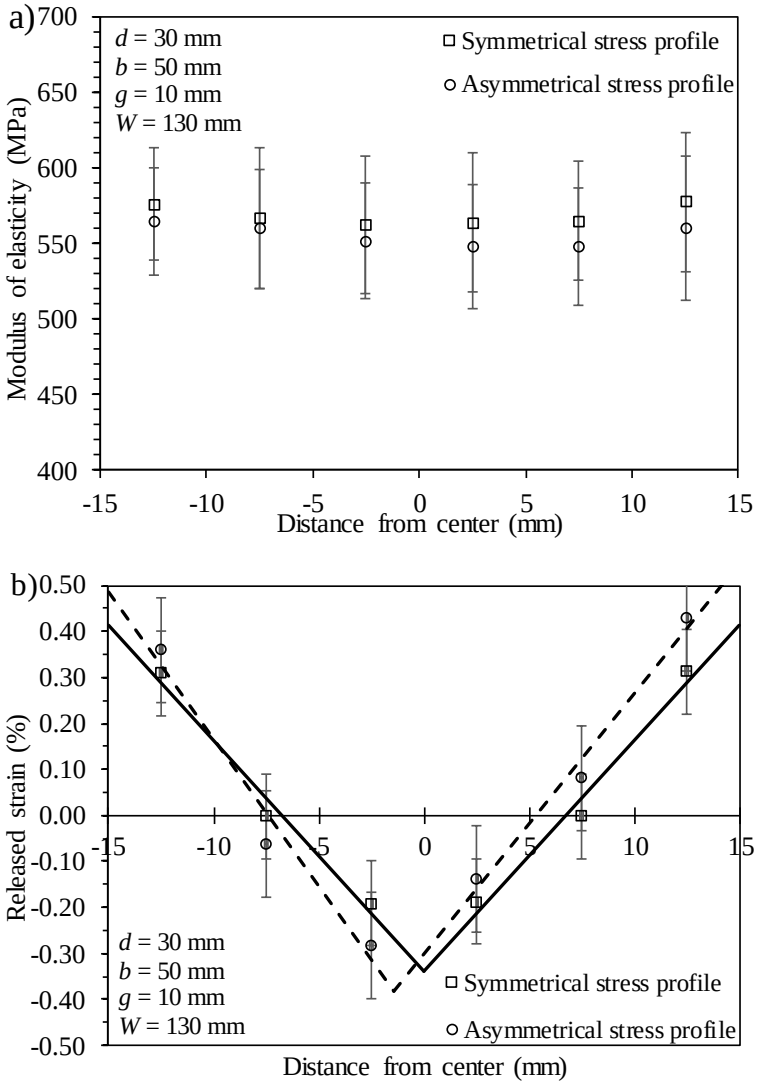

Figure 5: Profiles of a) modulus of elasticity and b) released strain plotted across the thickness of the specimens.

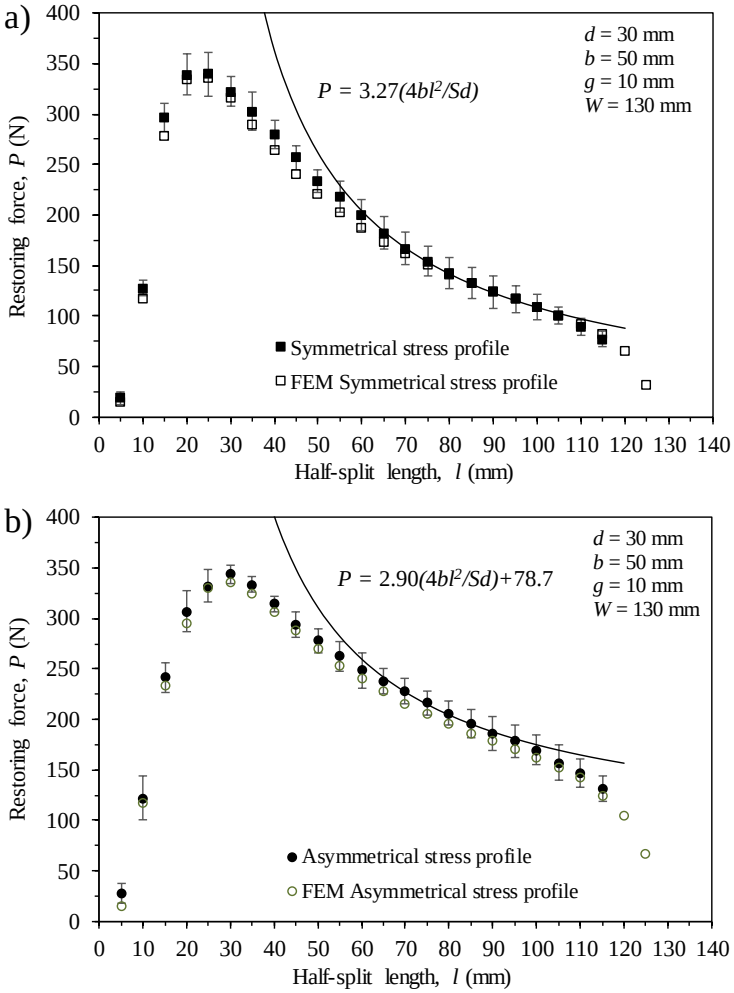

Figure 6: Comparison of experimental (symbols) and calculated restoring force (lines) profiles of the 30 mm thick half-split of a) the rare case ($P_o = 0$) and b) the typical case ($P_o \neq 0$).

4.3 The correlation of the stress profile deviation and the remnant force (P_o)

The FE model developed in the previous section was leveraged to investigate the effect of the stress profile deviation on the remnant force (P_o). The symmetric stress profile was initially generated by setting the maximum tensile stress of 1.0 MPa at the centre of the specimen and the maximum compressive stress of 1.0 MPa on both surfaces as presented by a solid black line in Fig. 7.

By moving the point of the maximum tensile stress from the centre, called the deviated distance *Xd*, the stress profile was changed from symmetry to asymmetry as shown by the coloured lines at the different deviated distances in Fig. 7. The compressive stresses on both surfaces were automatically calculated by the FE model. The maximum tensile stresses were slightly decayed less than 1.0 MPa while the maximum compressive stresses on the left surface were increased from 1.0 MPa with the decrease of the compressive stresses on the right surface. Although the stress levels of any deviated distances were different, the FE model still kept the calculation based on the equilibrium. The summation of tension force at the inner core always equals the compression force at the surfaces. The contours of the applied stress are demonstrated in Fig. 8.

The restoring force of all cases was calculated at cutting length from 5 mm to 125 mm at every 5 mm interval as shown in Fig. 9. By plotting the restoring force P versus the term $4bl^2/Sd$ in Eq. (6), the value of σ_m can then be determined from the slope of the graph and the remnant force P_o can also be deduced from the value of a positive y-intercept as shown in Fig. 10. For

the case of symmetric stress profile (circle dots), the restoring force calculated by FE well coincided with the restoring force derived from the beam theory in the flexural range with the vanishing of P_o. Due to the point of the maximum tensile stress deviating from the centre, the restoring force of the asymmetric cases is observed by moving up slightly at the short half-split length before reaching the maximum point and obviously increasing at the flexural regime.

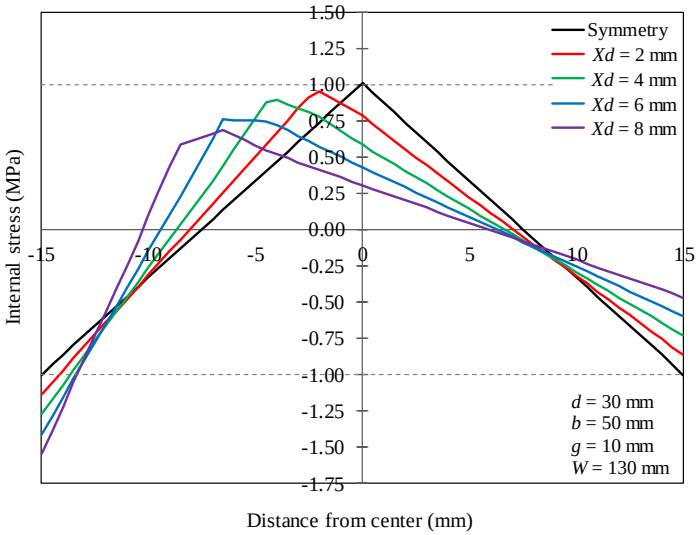

Figure 7: Stress profiles applied to FE model at various peak deviations (*Xd*) from 0 mm (symmetry), 2 mm, 4 mm, 6 mm, to 8 mm.

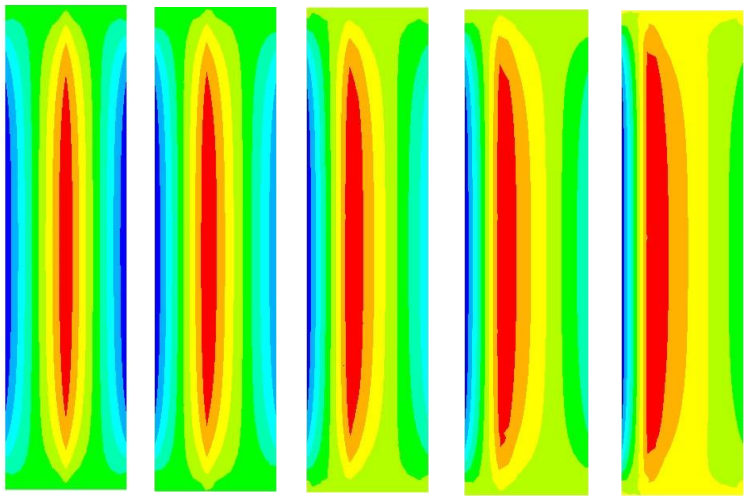

Figure 8: The contour of the internal stress of the symmetric case and the peak deviations of 2 mm, 4 mm, 6 mm and 8 mm.

By plotting the remnant force P_o versus the deviated distance *Xd* as presented in Fig. 11 a, one could find the linear relation between those two parameters. This means the value of the remnant force P_o depended on the stress deviation which is inferred to the level of asymmetric stress profile. The more the stress profile deviated, the larger remnant force was observed. However, the internal stresses of all asymmetric cases evaluated by Eq. (6) were less than the symmetric case of 1 MPa as plotted in Fig. 11 b. These stress values calculated from the restoring force from FE models may be the average value of the tensile stress at the inner layer with the compressive stress at the surfaces. Moreover, the internal stress in Eq. (6) originally derived from the symmetric case. Therefore, the complex equation of the restoring force for asymmetric stress profile is needed to be adapted and this will be a topic of future work.

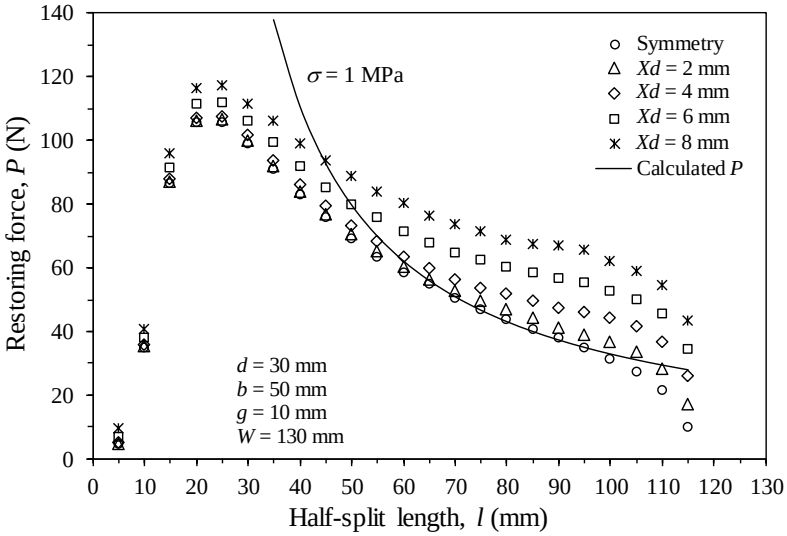

Figure 9: The effect of stress profile deviation on the restoring force P and the remnant force P_o.

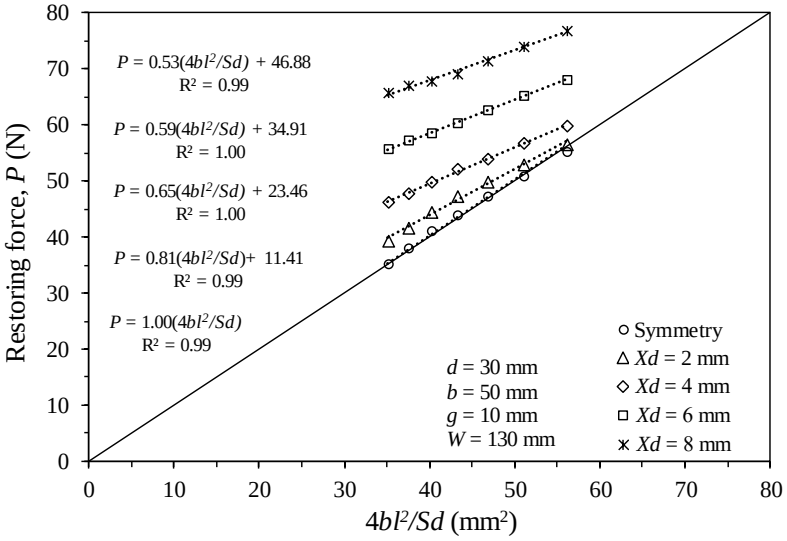

Figure 10: Plots of the restoring force P versus the term $4bl^2/Sd$ for the symmetric case and the peak deviations of 2 mm, 4 mm, 6 mm and 8 mm.

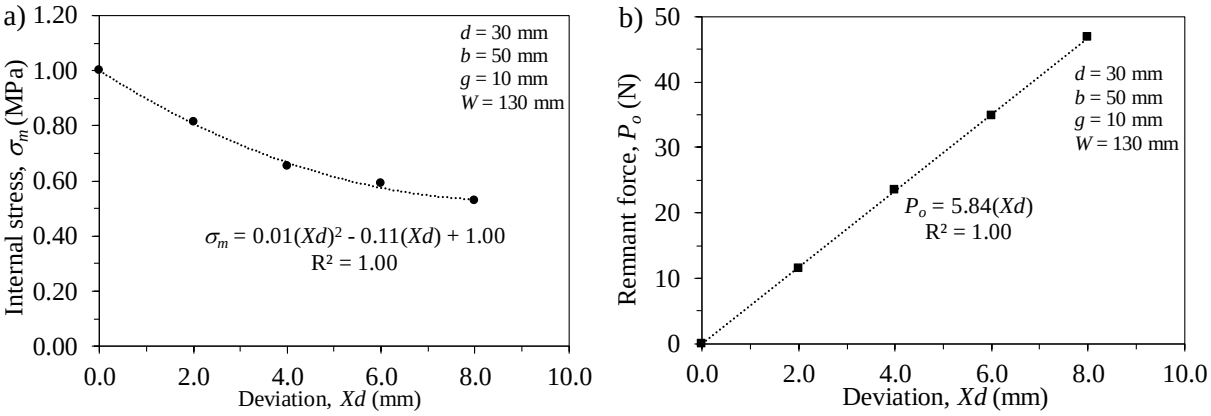

Figure 11: Plots of a) the remnant force P_o and b) the internal stress σ_m versus the stress profile deviation Xd.

5. CONCLUSION

The restoring force measured on a half-split specimen can be divided into two cases. The first one is relatively rare to find out which has only a force in the flexural range due to relaxation of the symmetric drying stress profile. In most cases, the restoring force of the second cases comprises of a force in the flexural range and a remnant force due to the asymmetric internal stress profile. Additionally, a numerical result based on the finite element model successfully simulates the restoring force profile for an entire range of both symmetric and asymmetric stress profiles by using the released strain and elastic modulus data in the tangential direction across the entire thickness obtained from the McMillen slice test. Moreover, the finite element model is leveraged to evaluate the effect of asymmetry of stress profile on the remnant force. The value of the remnant force linearly depends on the stress profile deviation which is inferred to the level of asymmetric stress profile. The more the stress profile deviated, the larger remnant force is generated.

Regarding this research study, the analytical model for describing the restoring force and a remnant force due to the asymmetric stress profile of wooden specimen should be derived as a future work. Additionally, some other stress profiles should be evaluated both in numerical model and analytical one compared with the linear profile. Another possible research project may focus on the application of the restoring force technique to measure the internal stress in other wood species and other materials such as steel and concrete.

ACKNOWLEDGEMENT

The first author wishes to thank the National Science and Technology Development Agency, Thailand, for supporting a graduate scholarship. The authors gratefully acknowledge the Thailand Science Research and Innovation and Walailak University for the financial support (Grant No. RSA6180077) and the National e-Science Infrastructure Consortium for providing computing resources that have partly contributed to the research results reported in this paper. Special thanks are reserved for Nakhon Si Parawood Co., Ltd., of Nakhon Si Thammarat, and Asia Pacific Parawood Co., Ltd., of Trang for providing the kiln-dried rubberwood boards used in this work.

REFERENCES

[1] Zhan, J.-F.; Avramidis, S. (2017). Impact of conventional drying and thermal post-treatment on the residual stresses and shape deformations of larch lumber, *Drying Technology*, Vol. 35, No. 1, 15-24, doi:10.1080/07373937.2016.1156123

[2] Salinas, C.; Chavez, C.; Ananias, R. A.; Elustondo, D. (2015). Unidimensional simulation of drying stress in Radiata Pine wood, *Drying Technology*, Vol. 33, No. 8, 996-1005, doi:10.1080/07373937.2015.1012767

[3] Perez-Pena, N.; Chavez, C.; Salinas, C.; Ananias, R. (2018). Simulation of drying stresses in Eucalyptus nitens wood, *BioResources*, Vol. 13, No. 1, 1413-1424, doi:10.15376/biores.13.1.1413-1424

[4] Hering, S.; Keunecke, D.; Niemz, P. (2012). Moisture-dependent orthotropic elasticity of beech wood, *Wood Science and Technology*, Vol. 46, No. 5, 927-938, doi:10.1007/s00226-011-0449-4

[5] Jiang, J.; Bachtiar, E. V.; Lu, J.; Niemz, P. (2017). Moisture-dependent orthotropic elasticity and strength properties of Chinese fir wood, *European Journal of Wood and Wood Products*, Vol. 75, No. 6, 927-938, doi:10.1007/s00107-017-1166-y

[6] Zhu, Z.; Buck, D.; Ekevad, M.; Marklund, B.; Guo, X.; Cao, P.; Zhu, N. (2019). Cutting forces and chip formation revisited based on orthogonal cutting of Scots pine, *Holzforschung*, Vol. 73, No. 2, 131-138, doi:10.1515/hf-2018-0037

[7] Diawanich, P.; Tomad, S.; Matan, N.; Kyokong, B. (2012). Novel assessment of casehardening in kiln-dried lumber, *Wood Science and Technology*, Vol. 46, No. 1-3, 101-114, doi:10.1007/s00226-010-0384-9

[8] Jantawee, S.; Leelatanon, S.; Diawanich, P.; Matan, N. (2016). A new assessment of internal stress within kiln-dried lumber using a restoring force technique on a half-split specimen, *Wood Science and Technology*, Vol. 50, No. 6, 1277-1292, doi:10.1007/s00226-016-0852-y
[9] Leelatanon, S.; Jantawee, S.; Vannarat, S.; Matan, N. (2019). Evaluation of the dyring stress in industrial kiln-dried boards using a force-based technique, *BioResources*, Vol. 14, No. 2, 4403-4412, doi:10.15376/biores.14.2.4403-4412
[10] Jantawee, S.; Leelatanon, S.; Diawanich, P.; Vannarat, S.; Matan, N. (2018). Comparison of techniques for quantification of internal stress within industrial kiln-dried lumber, *European Journal of Wood and Wood Products*, Vol. 76, No. 2, 617-627, doi:10.1007/s00107-017-1243-2
[11] Leelatanon, S.; Jantawee, S.; Vannarat, S.; Matan, N. (2020). Applications of Timoshenko beam theory and free edge effect for interpretation of stress in kiln-dried lumber using the restoring force technique, *Mechanics of Materials*, Vol. 150, Paper 103568, 11 pages, doi:10.1016/j.mechmat.2020.103568
[12] Walton, H. W. (2002). Deflection methods to estimate residual stress, Totten, G.; Howes, M.; Inoue, T. (Eds.), *Handbook of Residual Stress and Deformation of Steel*, ASM International, Novelty, 89-98
[13] Lados, D. A.; Apelian, D. (2006). The effect of residual stress on the fatigue crack growth behavior of Al-Si-Mg cast alloys – Mechanisms and corrective mathematical models, *Metallurgical and Materials Transactions A*, Vol. 37, No. 1, 133-145, doi:10.1007/s11661-006-0159-y
[14] Hibbeler, R. C. (2015). *Structural Analysis*, 9th edition, Pearson Prentice Hall, Upper Saddle River
[15] Rosnitschek, T.; Hueter, F.; Alber-Laukant, B. (2020). FEM-based modelling of elastic properties and anisotropic sinter shrinkage of metal EAM, *International Journal of Simulation Modelling*, Vol. 19, No. 2, 197-208, doi:10.2507/IJSIMM19-2-509
[16] Ray, T.; Kaljun, J.; Dolsak, B. (2021). Numerical model application to predict the sound quality of an instrument, *International Journal of Simulation Modelling*, Vol. 20, No. 4, 696-706, doi:10.2507/IJSIMM20-4-580
[17] Mentrasti, L.; Molari, L.; Fabiani, M. (2021). Poisson's ratio bounds in orthotropic materials. Application to natural composites: wood, bamboo and Arundo donax, *Composites Part B: Engineering*, Vol. 209, Paper 108612, 11 pages, doi:10.1016/j.compositesb.2021.108612
[18] Mascia, N. T.; Nicolas, E. A. (2013). Determination of Poisson's ratios in relation to fibre angle of a tropical wood species, *Construction and Building Materials*, Vol. 41, 691-696, doi:10.1016/j.conbuildmat.2012.12.014
[19] Perré, P.; Passard, J. (2007). Stress development, Ch. 11, Perré, P. (Ed.), *Fundamentals of Wood Drying*, A.R.BO.LOR., Nancy, 243-271